Research paper

Development of numerical code for physical hazard analysis of high-energy materials

Tei Saburi*†, Shiro Kubota*, Yuji Wada*, and Masatake Yoshida**

*Research Institute of Science for Safety and Sustainability, National Institute of Advanced Industrial Science and Technology, Onogawa 16−1,Tsukuba, Ibaraki 305−8569, JAPAN
Phone : +81−29−861−8760
†Corresponding address : t.saburi@aist.go.jp

**Explosion Research Institute Inc., MVK Bldg. 3F, Sotokanda 6−15−4, Chiyoda, Tokyo, 101−0021, JAPAN
Phone : +81−3−6803−2263

Received : February 25, 2013 Accepted : April 5, 2013

Abstract

We have developed a multidimensional analysis code for reactive shocks (MARS) for investigating various scenarios in the physical hazard analysis of high energetic materials. In this paper, details of numerical procedures in our code are presented. To confirm the reliability of the code, some of the one-dimensional test problems, shock tube, high velocity impact, propagation of blast wave and shock to detonation transition process, are solved. The previous our experiments, the gap tests are also simulated. By comparison of the experimental and numerical results, it was shown that the simulation can reproduce three typical results. The first case was that the shock to detonation transition occurs in acceptor, the second case was the no detonation but rapid decomposition occurs in acceptor and the third one was the detonation in acceptor occurs by the reflection of the shock wave at the interface of the acceptor and witness steel block. By the demonstration of reproducibility of the experimental result, it was shown that the code is generally applicable to the practical explosion problem.

Keywords : CFD code, CIP, reactive flow simulation, sympathetic detonation

1. Introduction

A computational fluid dynamics (CFD) simulation plays an important role in the field of explosion safety assessment of high energetic materials. We have developed the CFD code MARS[1)−3)] (multidimensional analysis code for reactive shocks) based on a CIP method[4)−6)], and adopted it for the investigation of many explosion-related problems[7)−10)]. The explosion phenomena of high energetic materials include ignition by an external stimulus, various types of detonation transition and propagation, the rapid expansion of detonation products, and the propagation of shock waves in various media. The peripheral materials are subjected to high-speed and large deformation, and destruction. The blast waves propagate far from the explosion source and interact with structures to damage them. Therefore, the code for physical hazard analysis should employ not only robust and high-speed algorithms but also various functions, such as the equations of state, the constitutive equations, the damage and the burn models. Although many numerical schemes and models of materials have been proposed and applied to various problems, many problems remain in simulations used in physical hazard analysis owing to the diversity of the phenomena. The combination of numerical schemes, algorithms and models of materials may be important, so we are working on the development of a simulation code.

In this paper, the development of a reactive flow simulation for the estimation of sympathetic detonations in gap tests is discussed. The governing equations, algorithm, treatment of the multi-material cell, and reactive flow simulation in our code are described in section 2. In section 3, we report the results of simple one dimensional calculations and reactive flow simulations of a gap test on a high energetic material. By comparison of the experimental and numerical results, it is shown that our code can reproduce the results of various gap tests.

2. Numerical procedure

2.1 Governing equations and algorithm

The governing equations of the multi-material flow[11),12)] are

$$\frac{\partial f^\alpha \rho^\alpha}{\partial t} + \vec{u}\cdot\nabla(f^\alpha\rho^\alpha) = -f^\alpha\rho^\alpha\nabla\cdot\vec{u} \tag{1}$$

$$\frac{\partial \vec{u}}{\partial t} + \vec{u}\cdot\nabla\vec{u} = -\frac{1}{\rho}\nabla(p+q) \tag{2}$$

$$\frac{\partial f^\alpha \rho^\alpha e^\alpha}{\partial t} + \vec{u}\cdot\nabla(f^\alpha\rho^\alpha e^\alpha) = -f^\alpha\rho^\alpha e^\alpha\nabla\cdot\vec{u} - m^\alpha(p+q)\nabla\cdot\vec{u} \tag{3}$$

$$\frac{\partial f^\alpha}{\partial t} + \vec{u}\cdot\nabla f^\alpha = f^\alpha\left(\frac{K}{K^\alpha}-1\right)\nabla\cdot\vec{u} \tag{4}$$

where superscript α denotes the component of the αth material, f is the volume fraction of the component, p is the pressure, q is the artificial viscosity, ρ is the density, e is the specific internal energy, and $\vec{u}$ is the velocity vector. K^α is the bulk modulus of the αth component, K is the equivalent bulk modulus of all the components, and m is the mass fraction of each component. Equations (1), (2), and (3), respectively correspond to the conservation of mass, momentum, and energy. The advection equation of the volume fraction, Equation (4), is obtained from Equation (1) and the assumption that the entropies of the individual components remain constant during the advection process.

The algorithm of the CIP[4)-6)] scheme is adopted in our code. The governing equations are solved with two steps in each cycle, similarly to the particle-in-cell (PIC)[13)] method. Because the same treatment is adopted for each governing equation, only the mass conservation equation will be shown below. The first step is a non-advection step and can be expressed as follows for mass conservation.

$$\frac{dF^\alpha}{dt} = -F^\alpha\nabla\cdot\vec{u} = g \tag{5}$$

Here, F^α is $f^\alpha\rho^\alpha$. Because the CIP requires the spatial derivatives of the physical quantities in each direction, the equations obtained by spatial differentiation of the governing equation for each direction should be solved.

$$\frac{dF^\alpha_{x_i}}{dt} = g_{x_i} - \vec{u}_{x_i}\nabla\cdot F^\alpha \tag{6}$$

The subscript x_i denotes the spatial derivative for the i direction. The second step is an advection step, which can be expressed as follows.

$$\frac{\partial F^\alpha}{\partial t} + \vec{u}\nabla\cdot F^\alpha = 0 \tag{7}$$

Because the final profile of F^α is calculated by Equation (5), Equation (7) can be solved using the spatial profile. The original concept of the CIP solver used to solve Equation (7) is that the spatial profile of physical quantities that consist of a discrete point in the calculation field is interpolated by cubic polynomial interpolation to improve the accuracy of the advection calculation. Because the spatial derivatives of the physical quantities in each direction are used during interpolation, the spatial derivatives are also solved by the equations obtained by the differentiating the governing equation. After the advection step, the pressure in each cell is determined using the EOS to complete the simulation cycle.

Owing to the large discontinuity resulting from undershoots and overshoots in the CIP method, ρ^α and e^α often take unrealistic values. In this case, the first-order upwind scheme is used locally instead to obtain the above variables.

2.2 Determination of the pressure at the multi-materials cell[11),12)]

If a one-component material is used in the cell, the pressure is simply calculated from the EOS for a single component, i.e., $P = P^\alpha(\rho^\alpha, e^\alpha)$. On the other hand, if several-component materials exist in the cell, the mechanical equilibrium for each component is assumed when determining the pressure. The following assumptions are employed in our code. The relaxation time is very short compared with the time step in the simulation. Although the volume fraction can change to attain equilibrium, the total volume and mass fraction are fixed. The process is isentropic. The relationship between the pressure in the multi-material cell and the increment in the pressure of each component can be written as

$$P = P^\alpha + \Delta P^\alpha = P^\alpha - \frac{\Delta f^\alpha}{f^\alpha}K^\alpha \tag{8}$$

Because of the assumption that the total volume does not change,

$$\sum \Delta f^\alpha = 0 \tag{9}$$

Finally, the pressure in the multi-material cell can be expressed as,

$$P = \sum P^\alpha f^\alpha / K^\alpha \times \left(\sum f^\alpha / K^\alpha\right)^{-1} \tag{10}$$

From the assumption that the process is isentropic, the bulk modulus of each component is

$$K^\alpha = -v^\alpha\left(\frac{\partial P^\alpha}{\partial v^\alpha}\right)_S = \rho^\alpha(c^\alpha)^2 \tag{11}$$

Here, subscript S denotes the entropy, v is the specific volume, and c is the sound velocity.

2.3 Reactive flow simulation for high energetic materials[14)]

It is difficult to determine the state quantities in partially reacted high energetic materials by considering the components of the intermediate products in detail during hydrodynamic computation. Partially reacted states have been regarded as simple mixtures of the unreacted and completely reacted states. The variable λ is defined to indicate the degree of decomposition of high energetic materials and corresponds to the mass fraction of the detonation products; $\lambda = 0$ corresponds to the unreacted state and $\lambda = 1$ corresponds to the completely reacted state. Various initiation models have been proposed. The ignition and growth model[15)] is one of the

most useful models and is used in our code to examine the sympathetic detonation. Its formulation is

$$\frac{d\lambda}{dt} = I\,(1-\lambda)^{2/9}\eta^4 + G\,(1-\lambda)^{2/9}\lambda^{2/3}P^z \qquad (12)$$

where $\eta = v_0/v - 1$. The parameters z, G, and I depend on the material properties. Equation (12) is solved using an algorithm similar to that used to solve the governing equations. The calculation of the pressure in the partially reacted state is different to that in the multi-material cell. It also requires the mixing law because the state is defined as a mixture of the reactant and detonation products.

The specific volume and internal energy of the reacting explosive can be represented by linear combinations of individual components, as shown below.

$$v = (1-\lambda)\,v_u + \lambda v_r \qquad (13)$$
$$e = (1-\lambda)\,e_u + \lambda e_r \qquad (14)$$

The third assumption is the mechanical equilibrium,

$$P = P_u(v_u, e_u) = P_r(v_r, e_r) \qquad (15)$$

Subscripts u and r indicate the solid reactant and gaseous product components, respectively. There are four unknown variables; the specific volumes and internal specific energies for both components. Another physical assumption, fourth assumption, is needed to complete the calculation. In particular, the assumption of thermal equilibrium has been used as a closed assumption. However, many assumptions have been adopted as closed assumptions. A major reason for using assumptions other than thermal equilibrium is that it is experimentally or theoretically difficult to obtain accurate information on the temperature of both the reactant and detonation products. Therefore, our code employs following assumption as the closed assumption :[16]

$$E_u/E_r = E_{uh}/E_{rs} \qquad (16)$$

where subscript h denotes the Hugoniot state.

3. Examples of simulation

3.1 One-dimensional test simulations

To confirm the reliability of our code, simple one-dimensional problems were simulated, the results of which are shown in Figures 1 to 3. The first problem is a shock tube[17] for an ideal gas as shown in Figure 3. The initial calculation field consists of high- and low-pressure regions with an extremely large difference in the internal energy. The initial density and internal energy are 1.0 and 1.5 for the left region, and 0.5 and 1.0^{-20} for right region, respectively. Total number of the cell is 200. Although these are very rigid conditions, the results of our code showed great consistency.

Figure 2(a) shows the results of the impact problem of aluminum and copper. EOS of both materials is the Mie-Grunisen form EOS with the Hugoniot reference line. Hugoniot was given by the relationship between the shock velocity and the particle velocity, and was referred from LASL Shock Hugoniot data[18]. Total number of the cell is 400. In Figure 2(a), it can be seen that the interaction problem of two different solid materials is accurately solved by our code.

Figure 2(b) shows the interaction of TNT detonation products gas and an ideal gas. The EOSs for the calculation are the Jones-Wilkins-Lee (JWL)[19)–21)] and the ideal gas EOSs. The explosion energy and initial solid-phase density of TNT are set for the initial conditions of the detonation products gas. Therefore, the initial difference between the pressures of TNT and air is 80,000-fold, and the initial difference between the densities is more than 1000-fold. Although the conditions in the simulation are very rigid, our code shows great consistency.

Because the analytical solution was not available for the initiation of high energetic materials, the results obtained using the Lagrangian code[14),22)–24)] and our code were compared as shown in Figure 3. The subject of this simulation was the impact problem of the aluminum vs. TNT that corresponds to the initiation of high energetic material. EOSs for unreacted and completely reacted state for TNT are Hugoniot porous model[25)] and JWL, respectively. The ignition and growth model was used for both calculations. For this problem, the Lagrangian code, which completely maintains the material boundary, is advantageous to the Euler coordinate system. However, from Figure 3, the difference between the results obtained using the Lagrangian code and our code is very small. The validity of our code has been confirmed for a system that includes multiple-materials and has severe initial conditions.

3.2 Reactive flow simulation (sympathetic detonation)

The subject of the reactive flow simulations in this paper is a numerical reproduction of our previous experiments[8),9)], i.e. the gap tests. The gap test has been done to estimate the sensitivity of high-energetic materials and is test of the sympathetic detonation. The configuration is illustrated in Figure 4 as a cross section of the axisymmetric system. Both the donor and acceptor charges are RDX-based explosives. The charges are placed in a PMMA pipe with 26 mm inner diameter and 2 mm thickness. The small PMMA plate is used to adjust the gap length, and the large plate also serves as a blast shield for the observation. The steel block was used as witness block. High speed photography was carried out during the gap test. Using the information of the luminescence at the surface of the acceptor holder, go/no go conditions of the acceptor were confirmed experimentally. Figure 5 shows a snapshot taken by high-speed photography when the detonation wave in the donor charge arrived at the gap material. A part of the experimental setup was shown.

The 2-dimensional axisymmetric system of MARS was used. The calculation field was configured according to experimental configuration as shown in Figure 4. The EOS for the unreacted component was obtained from this experimental data. For the detonation products, the Cheetah[26)] was used to calculate the JWL parameter. The purpose of this simulation is to construct a reactive flow

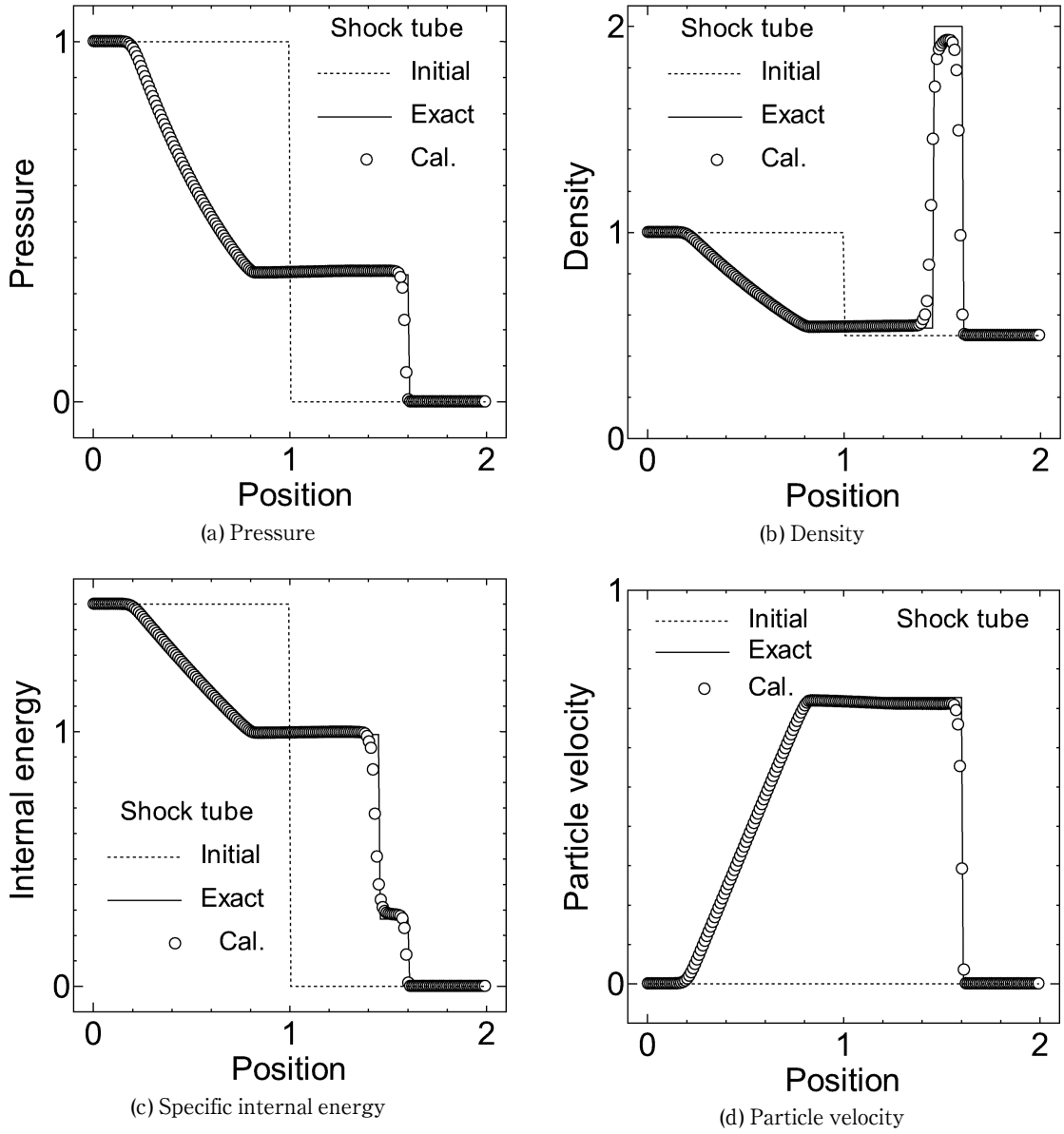

(a) Pressure (b) Density

(c) Specific internal energy (d) Particle velocity

Figure 1 Comparison of the numerical and theoretical results for the shock tube problem.

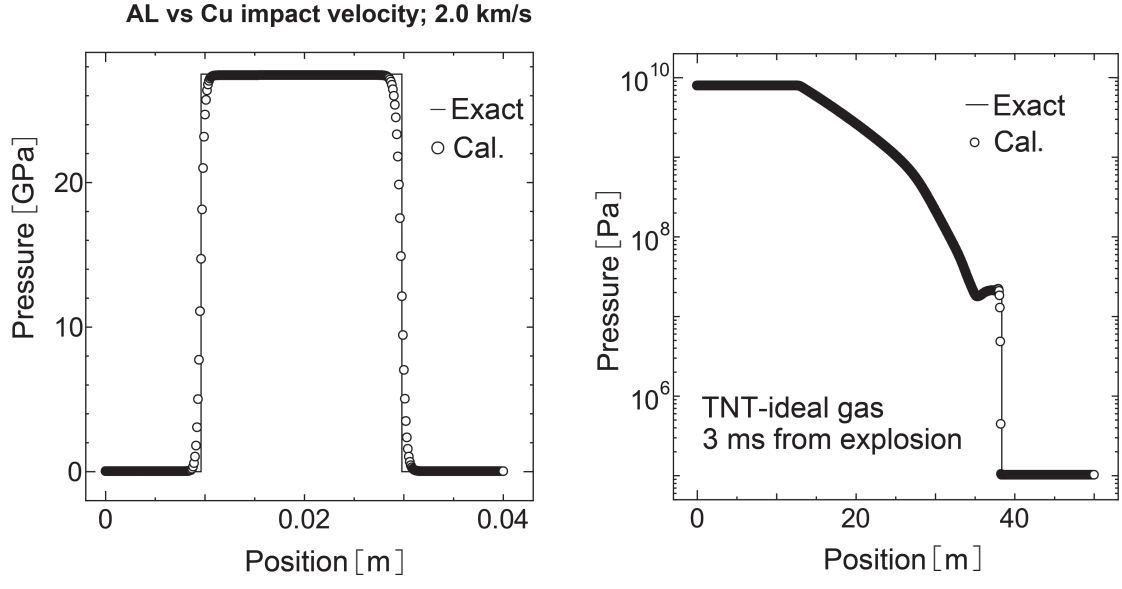

(a) Impact problem of Al and Cu (b) Expansion of TNT in air

Figure 2 Comparison of the numerical and theoretical results for the impact problem and the expansion process of TNT in air (pressure distribution).

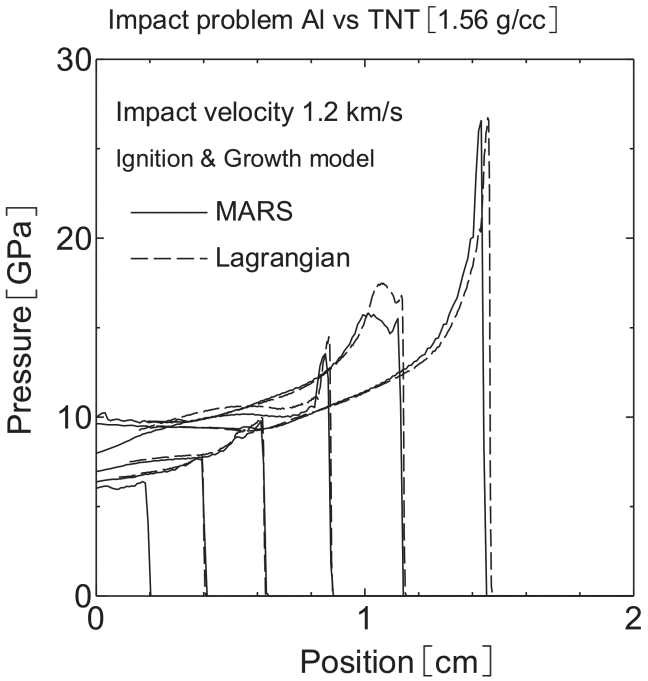

Figure 3 Comparison of the results for the Lagrangian code and our code for the impact problem of aluminum and TNT (shock initiation problem).

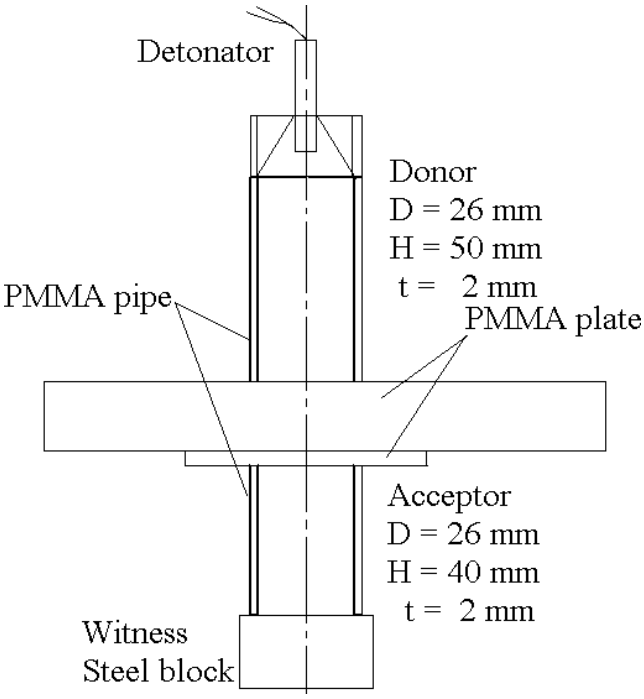

Figure 4 Configuration of the experimental setup for the gap test[8),9)]
(The subject of the reactive flow simulation)

simulation that can reproduce all the gap test results. The mesh size was set 0.5 mm. Comparisons of the result of high-speed photography and reactive simulations are shown in Figures 6 to 8. When the gap length was 22 mm, the acceptor charge was detonated from near the center as shown in Figure 6. In this figure, white portion in the acceptor indicates the high density region more than 1500 $kg \cdot m^{-3}$. This means that the detonation occurs in acceptor, and the white portion in acceptor corresponds to the detonation front. The calculation exhibits the density

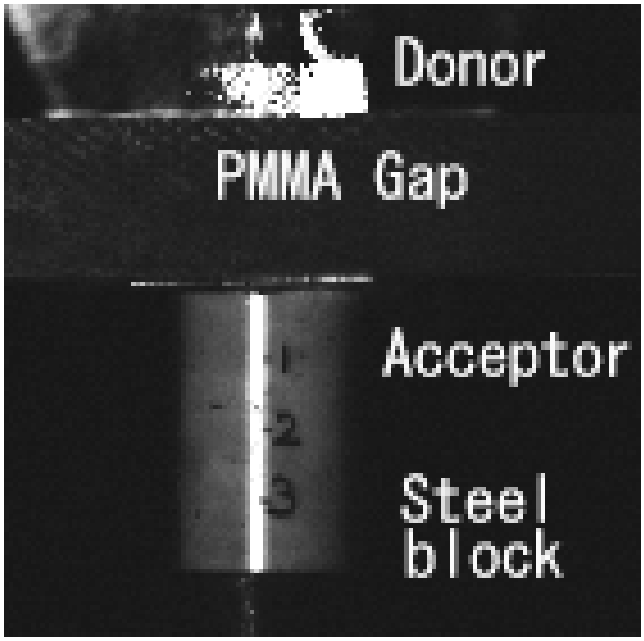

Figure 5 Snapshot taken by high-speed photography when the detonation wave in the donor charge arrived at the gap material (PMMA plate).

distribution inside explosive, which cannot be observed by experiment. A high density point, appears on the surface of the explosive (arrow in Figure 6(b)), was about 30 mm from the gap plate and was reasonably in consistency with the luminescence point at experiment (arrow in Figure 6 (a)). The simulation reproduced the gap test result of the go condition. When the gap length was 23 mm or longer, the detonation did not occur in the acceptor, and the 23 mm case is shown in Figure 7. In this case, although the setup is under the no go condition, immediately behind the shock front the acceptor charge rapidly expands in the radial direction with the decomposition of the charge. This observation was reproduced by our code. A start point of the expansion (arrow in Figure 7(b)) and a expanding shape outside the pipe were obtained in numerical simulation and were reasonably reproduce the experimental results. But a radial deforming velocity outside the PMMA pipe obtained in numerical simulation was slightly overestimated compared with that obtained in the experiment. In the case of a 23 mm gap length and 25 mm acceptor length, the results are shown in Figure 8. A rapid reaction was triggered by the reflection at the witness steel block. Because of the shorter length of the acceptor charge, the strength of the shock wave that arrived at witness block is greater than that in the above-mentioned case, so rapid reaction (detonation) occurs. The numerical simulation exhibits density profile inside the explosive and it was confirmed that the incidence of detonation was reproduced. The reactive flow simulation accurately reproduced the phenomena under three typical conditions.

4. Conclusions

Details of numerical procedures in our code were presented. Our code has employed governing equations for multi-material flow, which were solved by CIP

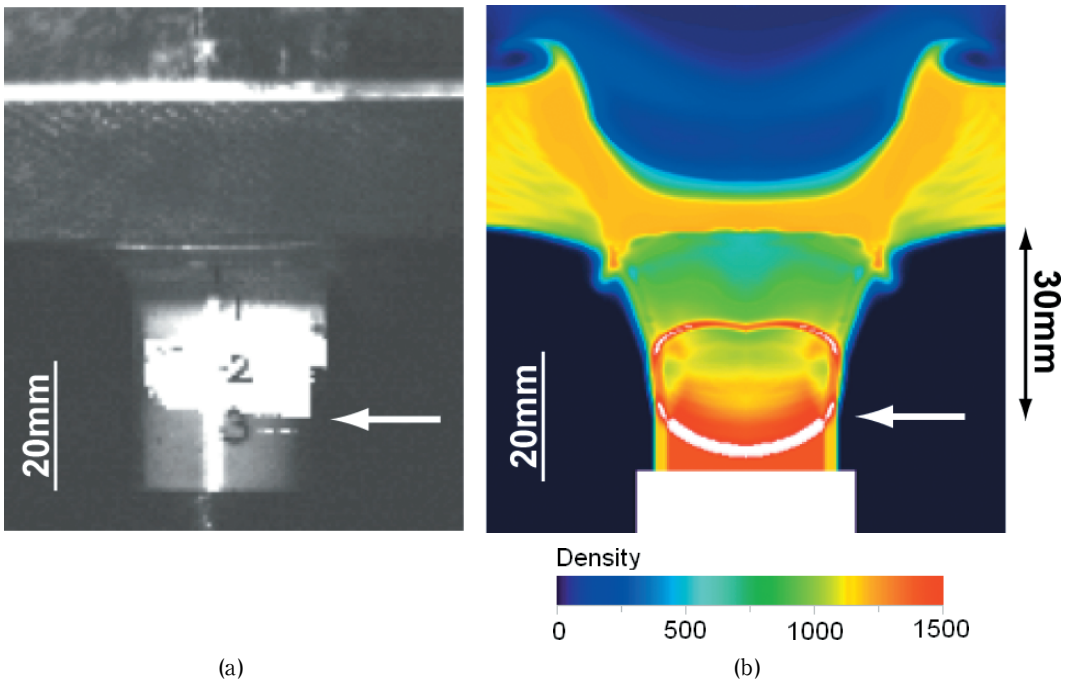

Figure 6 Comparison of the results of high-speed photography (a) and the reactive flow simulation (b); gap length 22 mm, length of acceptor 40 mm 20 us after initiation of donor, go condition. White color in simulation indicates the high density more than 1500 kg·m^{-3}.

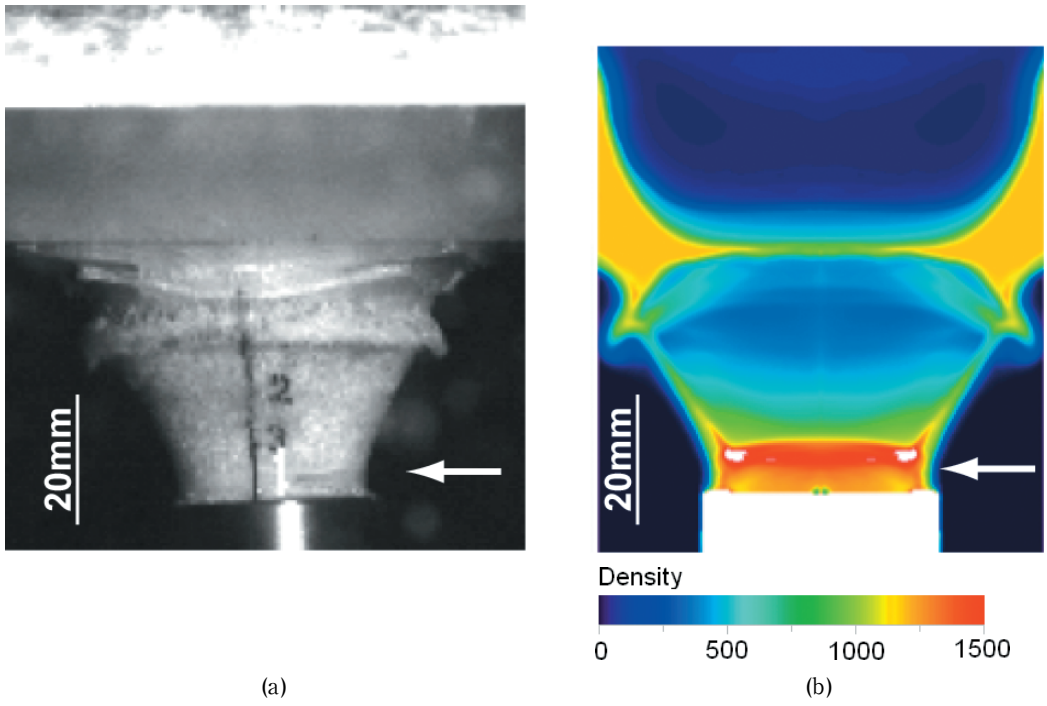

Figure 7 Comparison of the results of high−speed photography (a) and the reactive flow simulation (b); gap length 23 mm, length of acceptor 40 mm 37 us after initiation of donor, no go condition.

algorithm. It can apply to the reactive flow simulation. To confirm the reliability of the code, some of the one-dimensional test problems were solved. It was shown that the results of the exact and numerical solution are consistent. The previous our experiments, the gap tests were also simulated. By comparison of the experimental and numerical results, it was shown that the simulation could reproduce three typical results. Our developing code can be validly applied for physical hazard analysis of high energetic materials, especially the reactive flow problems.

References

1) Z. Liu, S. Kubota, M. Otsuki, K. Yoshimura, K. Okada, Y. Nakayama, M. Yoshida and S. Fujiwara, Kayaku Gakkaishi (Sci. Tech. Energetic Materials), 63, 264−270(2002).
2) Z. Liu, S. Kubota, M. Otsuki, D. Kim, Y. Nakayama and M. Yoshida, Mater. Sci. Forum, 465−466, 169−174(2004).
3) S. Kubota, Z. Liu, T. Saburi, Y. Ogata, and M. Yoshida, Proc. Computational Ballistics II, 107−114, WIT Press, Cordoba, Spain (2005).
4) H. Takewaki, and T. Yabe, J. Comput. Phys., 70, 355−372 (1987).

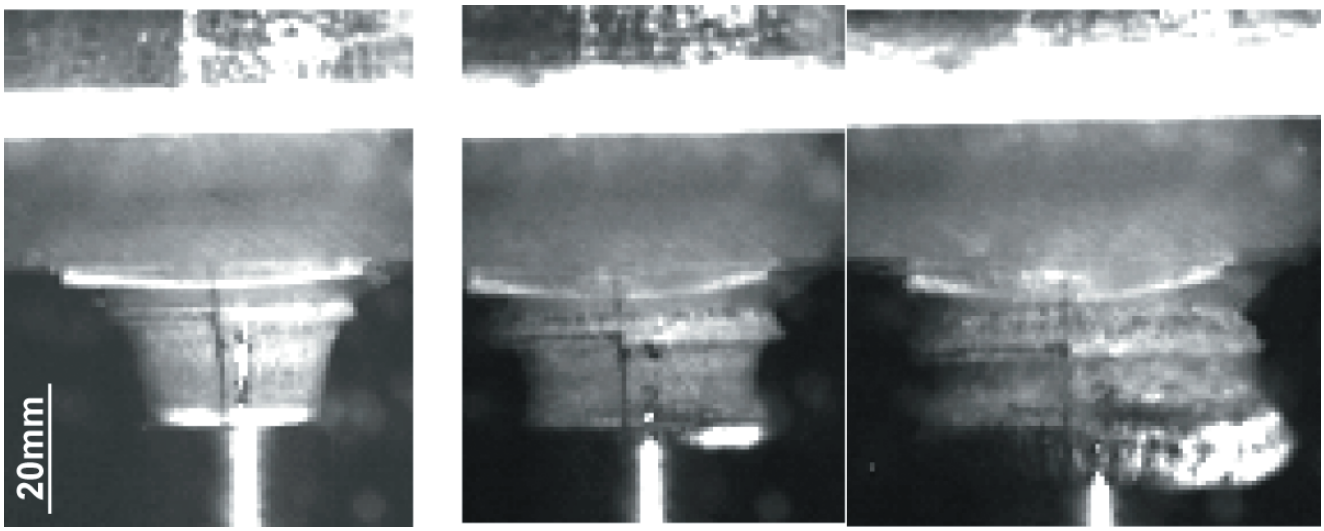

(a)

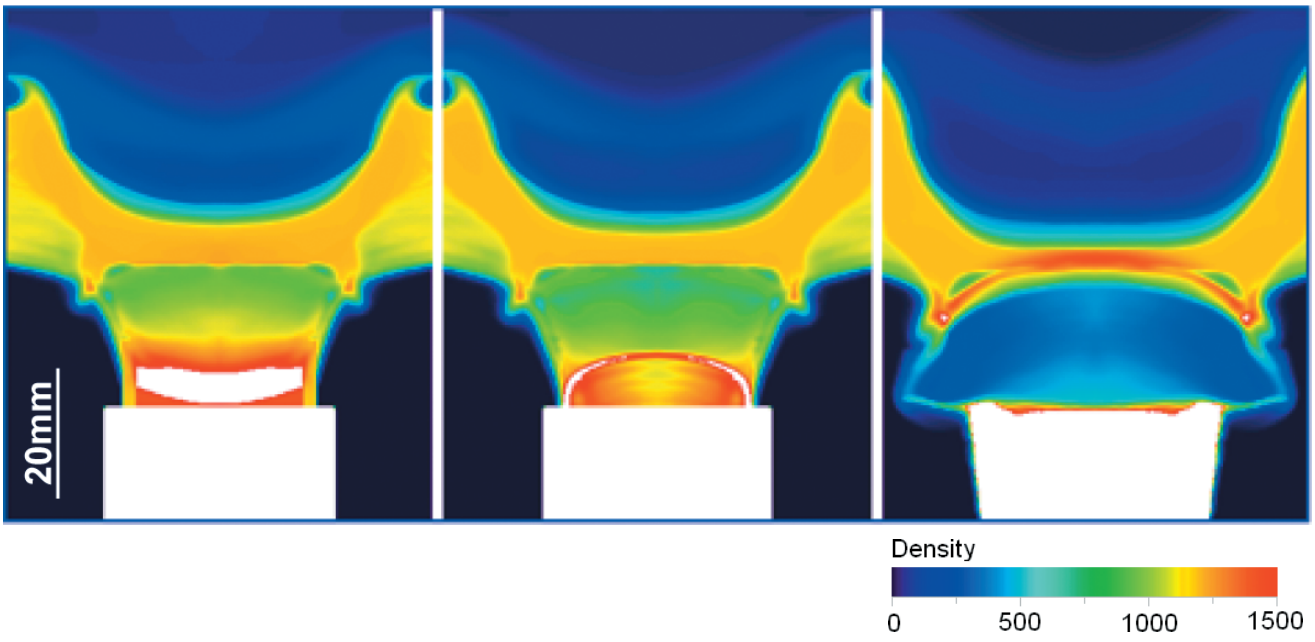

(b)

Figure 8 Comparison of the results of high-speed photography (a) and the reactive flow simulation (b); gap length 23 mm, length of acceptor 25 mm, time is counted from after the initiation of the donor.

5) T. Yabe, and T. Aoki, Comput. Phys. Commun., 66, 219–232 (1991).
6) T. Yabe, T. Ishikawa, P. Y. Wang, T. Aoki, Y. Kadota, and F. Ikeda, Comput. Phys. Commun., 66, 233–242(1991).
7) S. Kubota, Y. Ogata, Y. Wada, K. Katoh, T. Saburi, M. Yoshida and K. Nagayama, Proc. APS Topical Conf. on Shock Compression of Condensed Matter–2005, 1085–1088, APS Topical Group on SCCM, Baltimore (2005).
8) S. Kubota, Y. Ogata, Y. Wada, T. Saburi, M. Yoshida and K. Nagayama, Proc. 13thSymposium (International) on Detonation, 940–947, Norfolk, Office of Naval Research, Norfolk (2006).
9) S. Kubota, Y. Ogata, Y. Wada, K. Katoh, T. Saburi, M. Yoshida and K. Nagayama, Proc. APS Topical Conf. on Shock Compression of condensed matter–2007, 955–958, APS Topical Group on SCCM, Waikoloa (2007).
10) N. Kinoshita, S. Kubota, T. Saburi, Y. Ogata, and A. Miyake, Sci. Tech. Energetic Materials, 72, 21–25 (2011).
11) G. H. Miller, and E.G. Puckett, J. Comput. Phys., 128, 134–164 (1996).
12) O. Y. Vorobiev, and I. N. Lomov, "Numerical simulation of gas-solid interfaces with large deformations", Lawrence Livermore National Laboratory Report UCRL-JC-136868 (2000).
13) M. W. Evance and F. H. Harlow, "the Particle-in-cell Method for Hydrodynamic Calculations", Los Alamos Scientific Laboratory Report LA-2139 (1957).
14) S. Kubota, K. Nagayama, T. Saburi, and Y. Ogata, Combust. Flame, 151, 74–84 (2007).
15) E. L. Lee, and C. M. Tarver, Phys. Fluids 23, 2362(1980)
16) C. L. Mader, "Numerical Modeling of Detonations", University of California Press (1979).
17) G. A. Sod, J. Comput. Phys., 27,1–31 (1978).
18) S. P. Marsh, "LASL Shock Hugoniot data", University of California Press (1980).
19) J. W. Kury, H. C. Hornig, E. L. Lee, J. L. McDonnell, D. L.

Ornellas, M. Finger, F. M. Strange, and M. L. Wilkins, Proc. 4th Symposium (International) on Detonation, 3−13, Naval Ordnance Laboratory ACR-126, Washington DC (1965).
20) E. Lee, M. Finger, and W. Collins, "JWL Equation of State Coefficients for High Explosives", Lawrence Livermore National Laboratory Report UCID-16189 (1973).
21) B. M. Dobratz, "LLNL Explosives Handbook : Properties of Chemical Explosives and Explosives and Explosive Simulants", Lawrence Livermore National Laboratory Report UCRL-52997 (1981).
22) C. L. Mader and W. R. Gage, "Fortran SIN A One-Dimensional Hydrodynamic Code for Problems Which Include Chemical Reactions, Elastic-Plastic Flow, Spalling, and Phase Transitions", Los Alamos Scientific Laboratory Report LA-3720 (1967).
23) S. Kubota, T. Saburi, Y. Ogata, and K. Nagayama, Sci. Tech. Energetic Materials, 71, 44−50 (2010).
24) S. Kubota, T. Saburi, Y. Ogata, and K. Nagayama, Sci. Tech. Energetic Materials, 71, 92−97 (2010).
25) Ya. B. Zel'dovich and Yu. P. Raizer, "Physics of Shock Waves and High-Temperature Hydrodynamic Phenomena", Dover Publications (2002).
26) L. E. Fried, W. M. Howard, and P. C. Souers, "Cheetah 2.0 User's Manual"Lawrence Livermore National Laboratory UCRL-MA-117541 rev.5 (1998).

高エネルギー物質のフィジカルハザード評価のための数値解析コード開発

佐分利禎*†，久保田士郎*，和田有司*，吉田正典**

我々は高エネルギー物質のフィジカルハザード解析に関する様々なシナリオについて研究するために，反応衝撃波のための多次元解析コード（MARS）を開発している。この論文では，我々のコードにおける数値解析手法について述べる。数値解析コードの妥当性を検証するために，いくつかの１次元テスト問題（衝撃管，高速衝突問題，爆風，衝撃から爆轟への転移過程）を解いて，厳密解等と比較した。また，以前実施したギャップ試験の数値解析を実施した。実験と数値解析結果を比較した結果，数値解析は３つの典型的な結果を再現できることが分かった。すなわち，受爆薬中で爆轟が発生する場合，爆轟が発生しないが急速な分解が確認される場合，さらに受爆薬を伝播した衝撃波が金属製の証拠板で反射することで受爆薬中に爆轟が発生する場合である。実験再現性の検証により，解析コードは現実的な爆発問題への適用性を有することを示した。

独立行政法人産業技術総合研究所つくば西安全科学研究部門
*〒305−8569　茨城県つくば市小野川16−1
Phone : 029−861−8760
†Corresponding address : t.saburi@aist.go.jp

**〒101−0021　東京都千代田区外神田6−15−4MVKビル3F
株式会社爆発研究所